Physica B 477 (2015) 113–122

Contents lists available at ScienceDirect

Physica B

journal homepage: www.elsevier.com/locate/physb

Mössbauer spectroscopy, magnetic, and *ab initio* study of the Heusler compound Fe_2NiGa

Farshad Nejadsattari [a], Zbigniew M. Stadnik [a,*], Janusz Przewoźnik [b], Kurt H.J. Buschow [c]

[a] Department of Physics, University of Ottawa, Ottawa, Ontario, Canada K1N 6N5
[b] Solid State Physics Department, Faculty of Physics and Applied Computer Science, AGH University of Science and Technology, 30-059 Kraków, Poland
[c] Van der Waals-Zeeman Institute, University of Amsterdam, NL-1018 XE, The Netherlands

ARTICLE INFO

Article history:
Received 11 May 2015
Received in revised form
13 July 2015
Accepted 18 August 2015
Available online 20 August 2015

Keywords:
Mössbauer spectroscopy
Ferromagnet
Heusler compound

ABSTRACT

The structural, electronic, magnetic, elastic, and hyperfine-interaction properties of Fe_2NiGa have been determined by means of X-ray diffraction, ^{57}Fe Mössbauer spectroscopy, and magnetic measurements and *ab initio* calculations. The compound studied crystallizes in the cubic space group $F\overline{4}3m$ with lattice constant $a = 5.7961(4)$ Å. Evidence is provided for the presence of significant structural disorder in the compound. Fe_2NiGa is predicted to be half-metallic with covalent chemical bonding. It orders ferromagnetically with the Curie temperature $T_C = 586.0(7)$ K. The saturation magnetization per formula unit and the estimated Fe magnetic moments at the A and B sites are 3.00, 1.87(2), and 2.25(2) μ_B, respectively. The *ab initio* calculations overestimate the values of the A- and B-site Fe magnetic moments. It is observed that the magnetic properties of Fe_2NiGa are very strongly dependent on its heat treatment. The calculated hyperfine-interaction parameters show general agreement with the experimental ones. It is demonstrated that the compound studied decomposes when heated and kept at temperatures above around 500 K. The Debye temperature of Fe_2NiGa is found to be 378(5) K.

1. Introduction

Heusler compounds are a class of more than 1000 ternary intermetallic materials with composition X_2YZ or XYZ, where X and Y are transition metals and Z is a main group element [1]. They exhibit a rich variety of physical properties [2]. They occur as metals, semiconductors, or superconductors. These are compounds with different magnetic ordering. They possess shape-memory characteristics, exhibit heavy-fermion behavior, have giant magnetoresistance and enhanced thermoelectric properties. Some of them are topological insulators. Some of these properties have great potential for practical applications in, for example, spintronics or magnetocaloric technology.

Heusler compounds crystallize in the cubic space groups $Fm\overline{3}m$ or $F\overline{4}3m$. Within these two space groups, different types of atomic disorder, *i.e.*, various possible distributions of the X, Y, and Z elements among the specific crystallographic sites, are possible [3]. It is this disorder upon which the physical properties of the Heusler compounds are strongly dependent [2].

A subset of the Heusler compounds, Fe_2NiZ, is of current interest, especially from a theoretical point of view [4–10]. A few experimental studies of the Fe_2NiZ compounds have also been carried out [5,7,11–14]. Here we report the results of X-ray diffraction, ^{57}Fe Mössbauer spectroscopy, and magnetic study, complemented by first-principles electronic structure and hyperfine-interaction parameters calculations, of Fe_2NiGa.

2. Experimental and theoretical methods

An ingot of nominal composition Fe_2NiGa was prepared by arc melting the constituent elements of purity 99.9% in an atmosphere of purified argon. The ingot was then wrapped in a tantalum foil and vacuum-annealed at 1073 K for two weeks [14].

The X-ray diffraction (XRD) spectrum of Fe_2NiGa was measured at 298 K in Bragg–Brentano geometry on a PANalytical X'Pert scanning diffractometer using Cu $K\alpha$ radiation in the 2θ range 20–120° in steps of 0.02°. The $K\beta$ line was eliminated by using a Kevex PSi2 Peltier-cooled solid-state Si detector.

The dc magnetization was measured in the temperature range from 3.0 to 720 K and in magnetic fields up to 90 kOe using the vibrating sample magnetometer (VSM) option of the Quantum Design physical property measurement system (PPMS). The VSM oven option was used for dc magnetization measurements at temperatures higher than 400 K. The magnetic measurements were done on a solid Fe_2NiGa specimen in the form of a

* Corresponding author.
E-mail address: stadnik@uottawa.ca (Z.M. Stadnik).

http://dx.doi.org/10.1016/j.physb.2015.08.027
0921-4526/

parallelepiped.

The ^{57}Fe Mössbauer measurements were carried out using a standard Mössbauer spectrometer operating in sine mode and a ^{57}Co(Rh) source at room temperature. The spectrometer was calibrated with a 6.35-μm-thick α-Fe foil [15], and the spectra were folded. The Mössbauer absorber for low-temperature (<300 K) measurements consisted of a mixture of powdered Fe_2NiGa, and powdered boron nitride, which was pressed into a pellet and put into a high-purity, 8-μm-thick Al disk container to ensure a uniform temperature over the whole absorber. The Mössbauer absorbers for two series of high-temperature (>300 K) measurements were mixtures of powdered Fe_2NiGa and powdered boron nitride, that were placed into the solid boron-nitride containers. The low-temperature Mössbauer absorber was put into a Mössbauer cryostat in which it was kept in a static exchange gas atmosphere at a pressure of $\sim 7 \times 10^{-3}$ mbar. The high-temperature Mössbauer absorbers were put into a Mössbauer oven in which the dynamic pressure was $\sim 2 \times 10^{-5}$ mbar. The surface densities, σ_{exp}, of the prepared low-temperature/high-temperature Mössbauer absorbers were, respectively, 21.9, and 21.6, 33.0 mg/cm^2. These surface densities correspond to an effective thickness parameter [16] t_a in the range (5.9–9.0) f_a, where f_a is the Debye–Waller factor of the absorber. Since $t_a > 1$, the resonance line shape of the Mössbauer spectrum was described using a transmission integral formula [17].

Ab initio electronic structure and Mössbauer hyperfine-interaction parameter calculations have been performed within the framework of density functional theory using the full-potential linearized augmented-plane-wave plus local orbitals (FP-LAPW+lo) method, as implemented in the WIEN2k package [18]. In this method, one partitions the unit cell into two regions: a region of non-overlapping muffin-tin (MT) spheres centered at the atomic sites and an interstitial region. The wave functions in the MT regions are a linear combination of atomic radial functions times spherical harmonics, whereas in the interstitial regions they are expanded in plane waves. The basis set inside each MT sphere is split into a core and a valence subset. The core states are treated within the spherical part of the potential only and are assumed to have a spherically symmetric charge density in the MT spheres. The valence wave functions in the interstitial region were expanded in spherical harmonics up to $l=4$, whereas in the MT region they were expanded to a maximum of $l=12$ harmonics. For the exchange–correlation potential, the generalized gradient approximation (GGA) scheme of Perdew, Burke, and Ernzerhof [19] was used. A separation energy of –6.0 Ry between the valence and core states of individual atoms in the unit cell was chosen.

The values of 2.36 a.u., 2.36 a.u., and 2.30 a.u. were used as the MT radii for Fe, Ni, and Ga, respectively. The plane-wave cut-off parameter was set to $R_{MT} \times K_{MAX} = 7$, where R_{MT} is the smallest MT radius in the unit cell and K_{MAX} is the maximum K vector used in the plane-wave expansion in the interstitial region. A total number of 286 k-points was used within a $21 \times 21 \times 21$ k-mesh in the irreducible wedge of the first Brillouin zone. A convergence criterion for self-consistent field calculations was chosen in such a way that the difference in energy between two successive iterations did not exceed 10^{-4} Ry. The experimental lattice constant a in the space group $F\bar{4}3m$ (*vide infra*) was used in the calculations.

3. Results and discussion

3.1. Structural characterization

The room-temperature XRD pattern of Fe_2NiGa is shown in Fig. 1. Based on Burch's rule [20], it is expected that Fe_2NiGa should crystallize in the $F\bar{4}3m$ space group, *i.e.*, the Fe atoms should occupy the A (0,0,0) and B (0.25,0.25,0.25) sites, and the Ni and Ga atoms should occupy the C (0.5,0.5,0.5) and D (0.75,0.75,0.75) sites, respectively. A Rietveld refinement [20] of the XRD pattern in the $F\bar{4}3m$ space group (Fig. 1) yields the lattice constant $a = 5.7961(4)$ Å. The absence of the (111) and (002) *fcc* superstructure Bragg peaks in the experimental pattern (Fig. 1) is indicative that the studied Heusler compound is not well ordered, *i.e.*, some structural disorder (possible random occupation of the constituent elements in the available crystallographic sites) must exist in the compound. As has been noticed earlier [2], it is virtually impossible to determine the type of disorder in Heusler compounds using only the standard XRD technique.

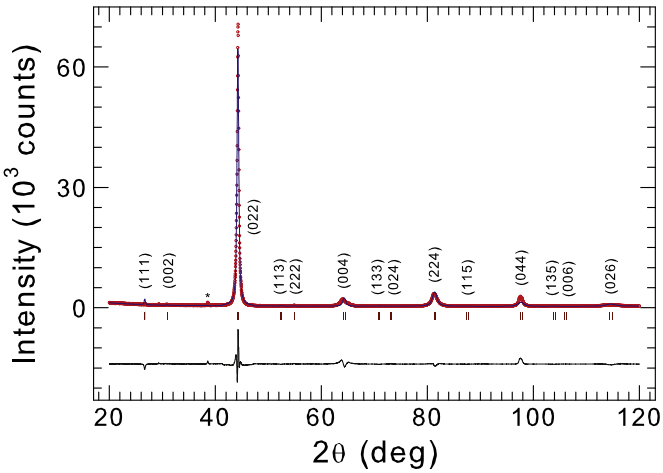

Fig. 1. X-ray diffraction pattern of Fe_2NiGa at 298 K. The experimental data are denoted by open circles, while the line through the circles represents the results of the Rietveld refinement. The row of vertical bars shows the indexed Bragg peak positions for the $Fm\bar{3}m$ space group. The symbol ∗ indicates the Bragg peak position corresponding to an unidentified impurity phase. The lower solid line represents the difference curve between experimental and calculated patterns.

The crystal structure of Fe_2NiGa in the $F\bar{4}3m$ space group is shown in Fig. 2. The presence of covalent bonding (*vide infra*) is indicated pictorially by rods in the unit cell (Fig. 2).

3.2. Ab initio calculations

3.2.1. Charge density distribution

Fig. 3 shows the calculated valence charge density distribution in the (110) and (100) planes in Fe_2NiGa. One observes a high degree of electron charge localization around the Ni and FeA (Fe

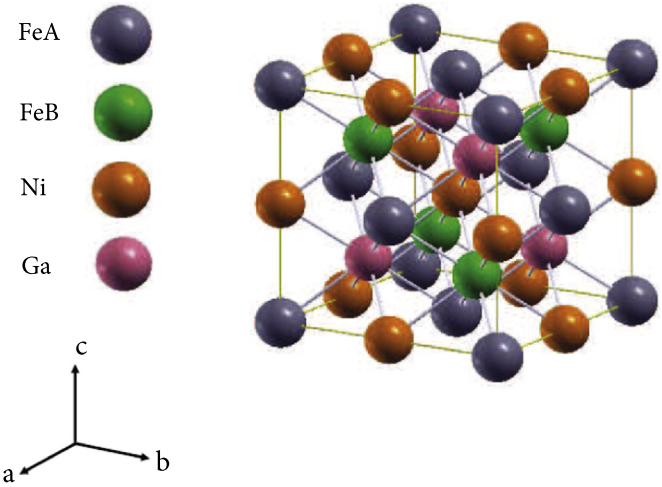

Fig. 2. The unit cell of the Fe_2NiGa compound in the $F\bar{4}3m$ space group.

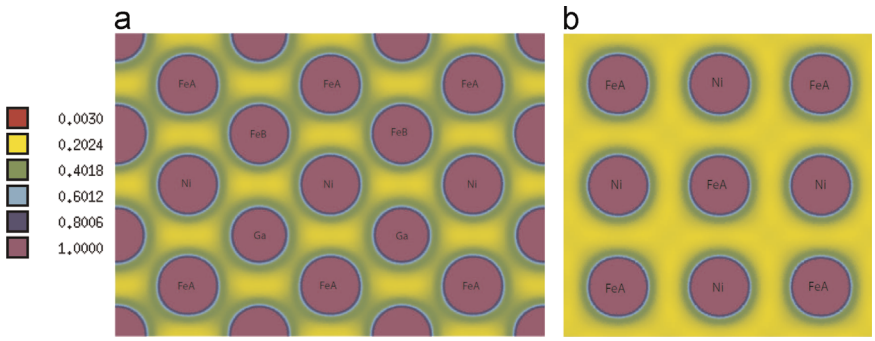

Fig. 3. Electron charge density distribution (in units of e/Å^3) in the (110) plane (a) and the (100) plane (b).

atoms at the A site) atoms in the (100) plane [Fig. 3(b)] and relatively large low-density (yellow-red) regions between these atoms. Consequently, there is rather weak covalent bonding between the Ni and FeA atoms. However, for the charge density distribution in the (110) plane [Fig. 3(a)], one finds that the electron charge is less localized which leads to shrinking of the low-density regions. As a result, a directional covalent bonding between the neighboring Fe and Ga, and Fe and Ni, atoms is formed. The nature of the covalent bonding between the Fe and Ga atoms is due to *p*–*d* hybridization.

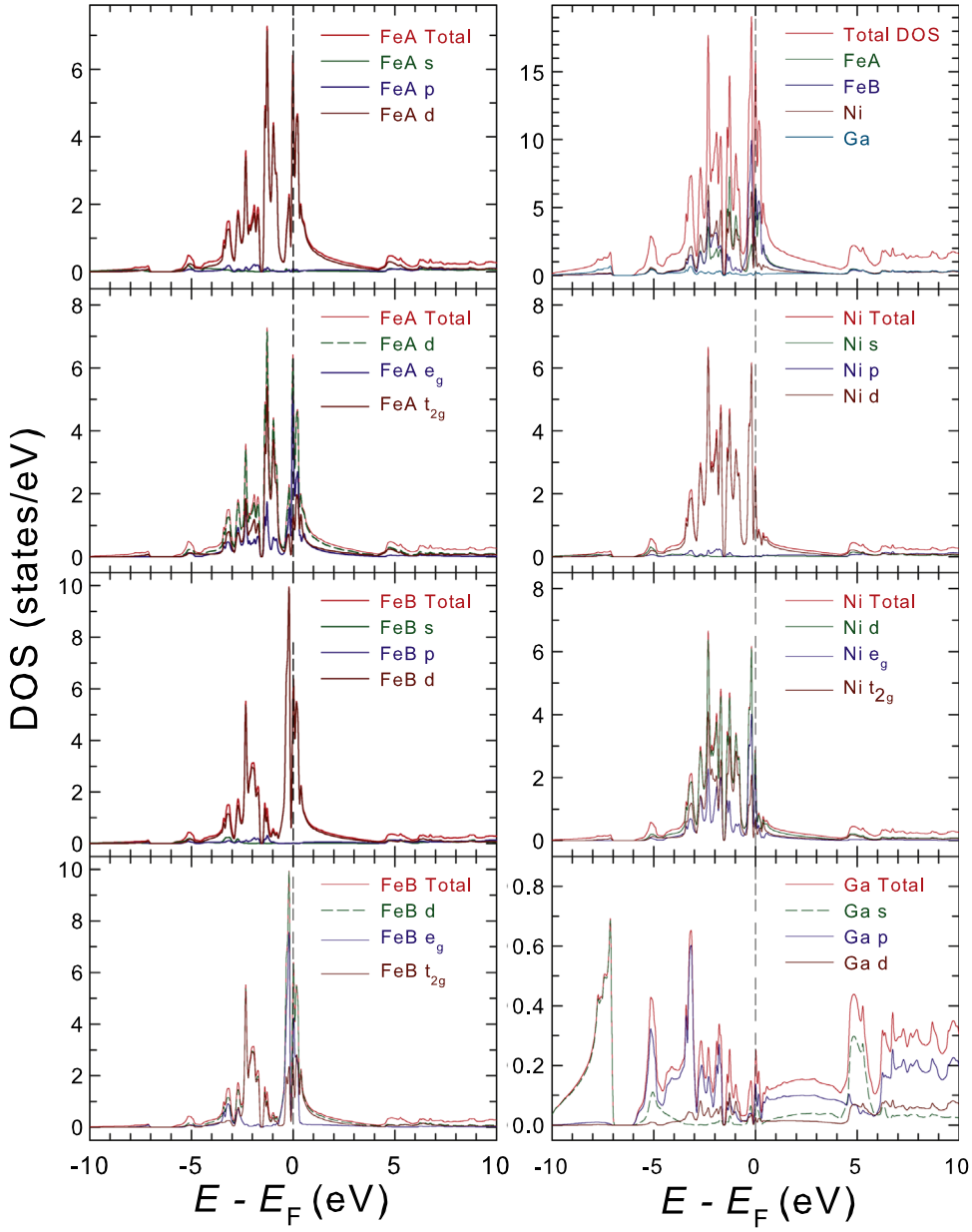

Fig. 4. Total, atom-, and orbital-resolved density of states of Fe_2NiGa in the nonmagnetic state.

By comparing the valence electron configuration of Ga with that of Fe and Ni, one expects the formation of *p*--*d* covalent bonds in which two electrons (from each of two Fe atoms) from 3*d* states along with three electrons from the Ni 3*d* states join the 4*p* states of Ga, forming relatively strong covalent bonds. One can also argue that, because the neighboring atoms in the (100) plane are on average further apart than the ones in the (110) plane, the electrons in the (100) plane are less likely to participate in forming bonds (Fig. 2). The Coulomb interaction between the neighboring atoms in the (100) plane is not large enough (due to their relatively large separation) to overcome the atomic binding of the electrons to their nuclei, which results in the localization of the electrons around their parent atoms. However, in the (110) plane the atoms are relatively closer to each other, and therefore the interaction between the nucleus of one atom and the electrons of the neighboring atom is large enough to form strong covalent bonds.

3.2.2. Nonmagnetic and ferromagnetic states

The nonmagnetic state of Fe_2NiGa refers to a high-temperature regime in which thermal agitations are strong enough to overcome any preferred magnetic ordering. Fig. 4 shows the total, atom-, and orbital-resolved density of states (DOS) of Fe_2NiGa in the non-magnetic state. One notices a large concentration of electronic states around the Fermi energy (E_F), which gives rise to good thermal and electrical conductivities. One can also notice (Fig. 4) a high degree of overlap of electronic states around E_F. This leads to chemical bonding of the covalent type. The dominant contribution to the DOS comes from the 3*d* states of FeB (Fe atoms at the B site) and Ni. The contributions of the Ga *s* and *p* states, which are peaked, respectively, at around 7 and 3.5 eV below E_F (Fig. 4), are very small.

The DOS for the e_g and t_{2g} states of FeA, FeB, and Ni has also been calculated (Fig. 4). As expected, the e_g states lie higher in energy than the t_{2g} states. For Ni, the e_g states extend from about 3.5 eV below E_F to the immediate vicinity of E_F and are peaked at 0.5 eV below E_F, whereas the t_{2g} states are peaked at around 2.5 eV below E_F. The location of these states for FeB is quite similar. Thus, both the e_g and t_{2g} states are not localized, *i.e.*, they are spread in energy below E_F.

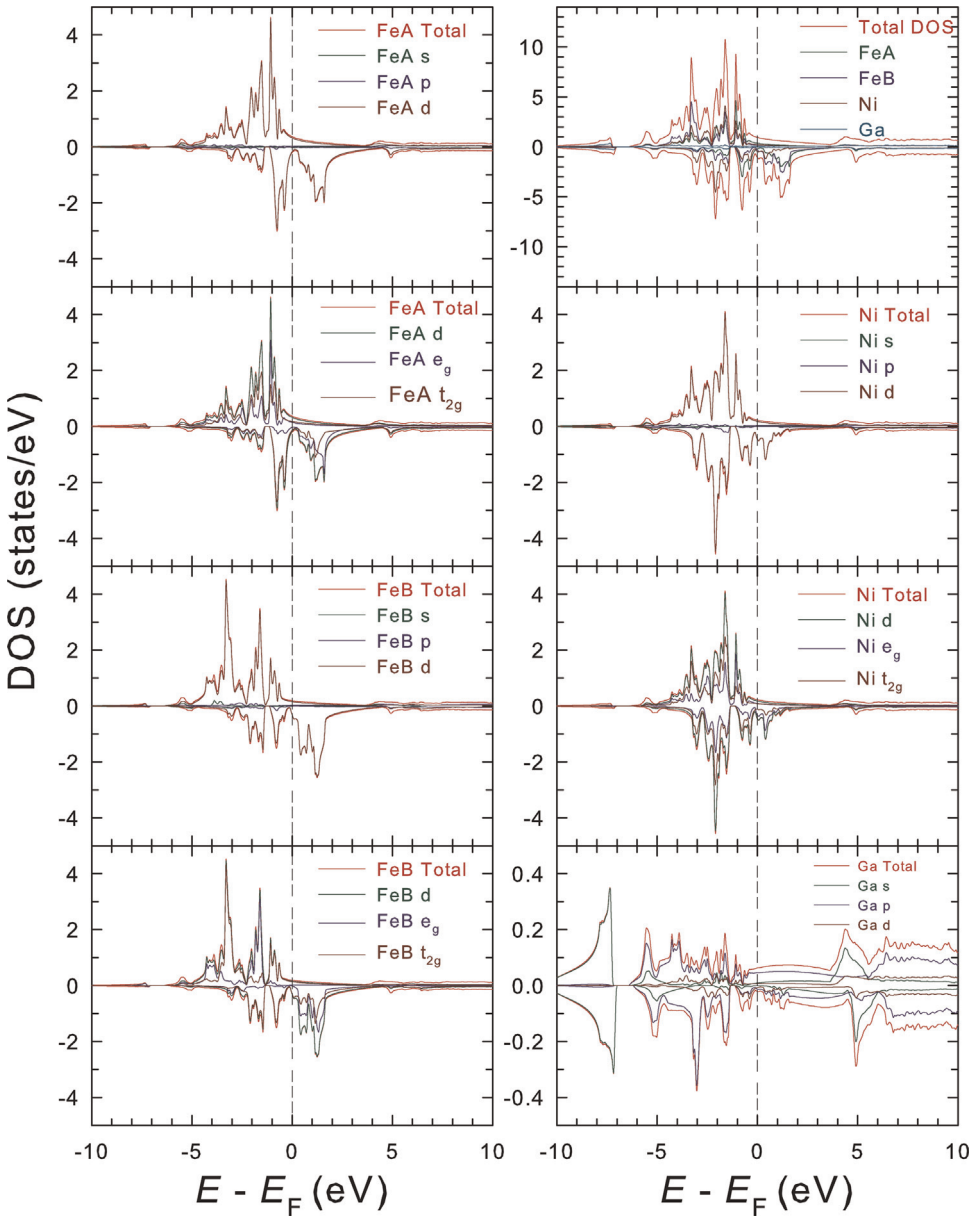

Fig. 5. Spin-polarized total, atom-, and orbital-resolved density of states of Fe_2NiGa in the ferromagnetic state.

By examining the band structure of Fe_2NiGa in the nonmagnetic state [Fig. 6(a)], one observes a large number of accessible states at and below E_F. These states are localized in energy, as compared to other states lower in energy, in all directions of the Brillouin zone and they are dominated by the Fe and Ni *d* states. One can also notice [Fig. 6(a)] a rather high density of conduction bands in the energy region between about 4 and 7 eV above E_F.

The spin-polarized total, atom-, and orbital-resolved DOS of Fe_2NiGa in the ferromagnetic state is shown in Fig. 5. For each spin configuration, the DOS is dominated by the Fe and Ni *d* states. For the spin-up configuration, these states are spread in the energy region from about 1 to 4.5 eV below E_F, *i.e.*, they are almost absent in the vicinity of E_F. This leads to the formation of a gap above E_F. However, for the spin-down configuration (Fig. 5), these states are spread between about −4 and 2 eV with respect to E_F. Thus, there is a rather high concentration of accessible spin-down states at E_F. These characteristics are reminiscent of half-metallic behavior, a behavior that can have important implications in the fields of spintronics where one considers spin-dependent currents. The spin-up electrons face a potential barrier and are blocked, whereas the spin-down current can freely flow. This creates a spin filter, or a spin switch, that can be used in quantum computation whereby the traditional bits "0" and "1" are replaced by the spin-dependent currents.

One also observes (Fig. 5) that the *d* states of FeA and FeB are the main contribution to the DOS, both for spin-up and spin-down configurations. Regarding the spin-up configuration, the FeA *d* states are widely spread from −4 to −1 eV with respect to E_F and are highly peaked around −1 to −1.5 eV. The FeB states, however, are strongly peaked at −1.5 and −3.3 eV. In the case of spin-down configuration, the FeA *d* states occupy a region from −2 to 2 eV in energy with respect to E_F and are strongly peaked at −1 to 1 eV. A similar pattern is observed for FeB *d* states but with a smaller concentration of DOS below E_F.

Within the Fe *d* states, the e_g states are peaked closer to E_F, whereas the t_{2g} states are distributed over lower energies, similar to the situation observed in the nonmagnetic state (Fig. 4). For both the spin-up and spin-down configurations the contributions of the e_g and t_{2g} states are of almost the same weight. The DOS arising from the Ni *d* state is different from that of the Fe *d* states in the sense that the main contribution of the *d* states for the spin-up configuration is mainly of the e_g type and is concentrated between about 1 and 1.8 eV below E_F. However, for the spin-down configuration the dominant contribution of the Ni *d* states is peaked at about 2 eV below E_F and is mainly of the t_{2g} type. The separation of spin-up and spin-down DOS for Fe and Ni leads to nonzero Fe and Ni magnetic moments. This is a direct result of the unfilled 3*d* shells in both atoms. As one can see from the bottom graph in Fig. 5, the total contribution of Ga to the overall DOS is negligibly small. More importantly, the states in both spin-up and spin-down configurations are distributed in a similar way. This accounts for the fact that the value of the Ga magnetic moment is close to zero. The calculated magnetic moments $\mu_{Fe}(A)$, $\mu_{Fe}(B)$, μ_{Ni}, and μ_{Ga} in the ferromagnetic state of Fe_2NiGa are 1.941, 2.680, 0.492, and $-0.054\,\mu_B$, respectively. The fact that $\mu_{Fe}(B)$ is larger than $\mu_{Fe}(A)$ can be deduced by inspecting Fig. 5. One observes that the difference in the distribution of the FeB *d* states between spin-up and spin-down configurations is larger than that of the FeA *d* states. The calculated magnetic moment per formula unit μ_{fu} is $4.958\mu_B$ [21].

The spin-polarized band structure of Fe_2NiGa is shown in Fig. 6 (b) and (c). The spin-up band structure shows an energy gap below E_F, while the spin-down band structure does not exhibit such a gap. One observes a large number of accessible states around E_F in the spin-down band structure [Fig. 6(c)], whereas in the spin-up band structure [Fig. 6(b)] there are only a few bands around E_F. This gives rise to a nearly half-metallic behavior as discussed earlier.

3.2.3. Elastic parameters

The elastic parameters discussed here were calculated for the optimized lattice constant of 5.7646 Å derived from the structural optimization of Fe_2NiGa (Fig. 7). The calculated density ρ of Fe_2NiGa is 8.1903 g/cm^3. For the cubic structure of Fe_2NiGa, the calculated second-order elastic constants [22] C_{11}, C_{12}, and C_{44} are 233.04, 196.20, and 175.40 GPa, respectively.

Using the calculated values of ρ and the elastic constants, one finds longitudinal and transverse sound velocities $(v_l = [(G_1 + 0.4(2C_{44} + G_2 - G_1))/\rho]^{1/2},\ v_t = [(C_{44} - 0.2(2C_{44} + G_2 - G_1))/\rho]^{1/2})$ of 6624.5 and 3712.1 m/s, respectively. This allows one to calculate the Debye temperature from the expression [22] $\Theta_D = h/k_B(3nN_A\rho/4\pi M)^{1/3}v_m$, where h is the Planck constant, k_B is the Boltzmann constant, n is the number of atoms per formula unit, N_A is the Avogadro constant, M is the molecular weight of the compound, and v_m is the average sound velocity $(v_m = [1/3(2/v_t^3 + 1/v_l^3)]^{-1/3})$. The calculated Θ_D is 427 K. We also calculated the equilibrium bulk modulus $B_0 = 204.2$ GPa.

3.2.4. Hyperfine-interaction parameters

Numerical analysis of Mössbauer spectra yields the three most

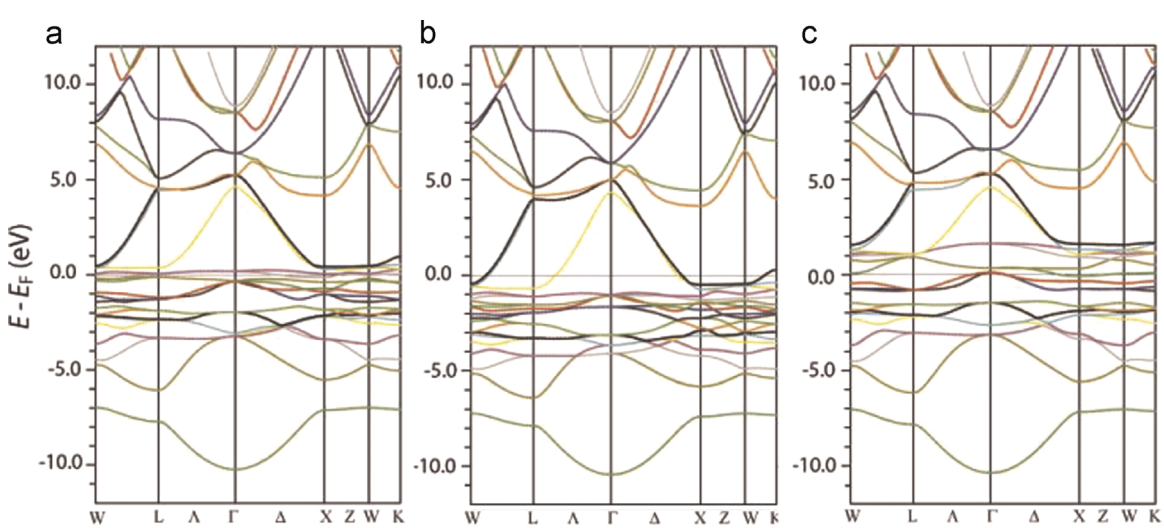

Fig. 6. (a) Energy band structure of Fe_2NiGa in the nonmagnetic state. (b) Spin-up and (c) spin-down band structures of Fe_2NiGa in the ferromagnetic state.

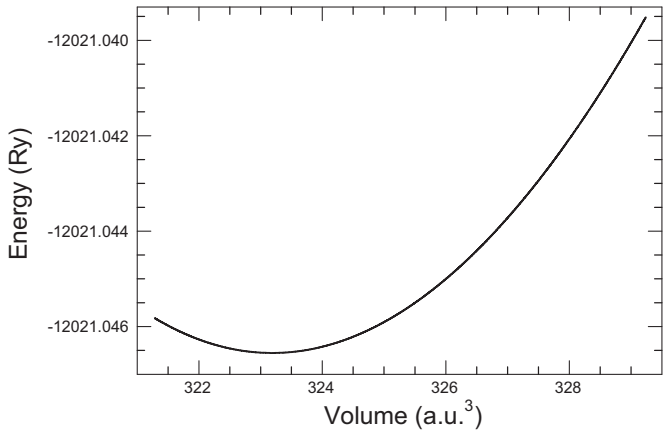

Fig. 7. Total energy as a function of primitive cell volume in the *fcc* structure of Fe_2NiGa.

important hyperfine-interaction parameters: the isomer shift, δ_0, the hyperfine magnetic field, H_{hf}, and the principal component of the electric field gradient (EFG) tensor, V_{zz}, with the asymmetry parameter, η [16]. If the crystal structure of a compound studied is known, these parameters can be also obtained from first-principles calculations [23]. For the compound studied here, the Fe atoms are located at the sites with the point symmetry $\bar{4}3m$, which ensures a vanishing EFG tensor.

The isomer shift results from the difference in the total electron density at the Mössbauer nucleus in the compound studied, $\rho(0)$, and in the reference compound, $\rho_{ref}(0)$,

$$\delta_0 = \alpha(\rho(0) - \rho_{ref}(0)), \tag{1}$$

where α is a calibration constant. In calculating $\rho(0)$, relativistic spin-orbit effects were invoked in order to account for the possibility of the penetration of the $p_{1/2}$ electrons into the ^{57}Fe nuclei. An α-Fe (with the *bcc* structure and the lattice constant of 2.8665 Å) was chosen as a reference compound. The calculated value of $\rho_{ref}(0)$ is 15309.918 a.u.$^{-3}$. The calculated values of $\rho(0)$ at the A and B sites are 15308.677 and 15309.300 a.u.$^{-3}$, respectively. Using the calibration constant $\alpha = -0.291$ a.u.^{3} (mm/s) (Ref. [24]), Eq. (1) gives $\delta_0(A) = 0.361$ mm/s and $\delta_0(B) = 0.180$ mm/s.

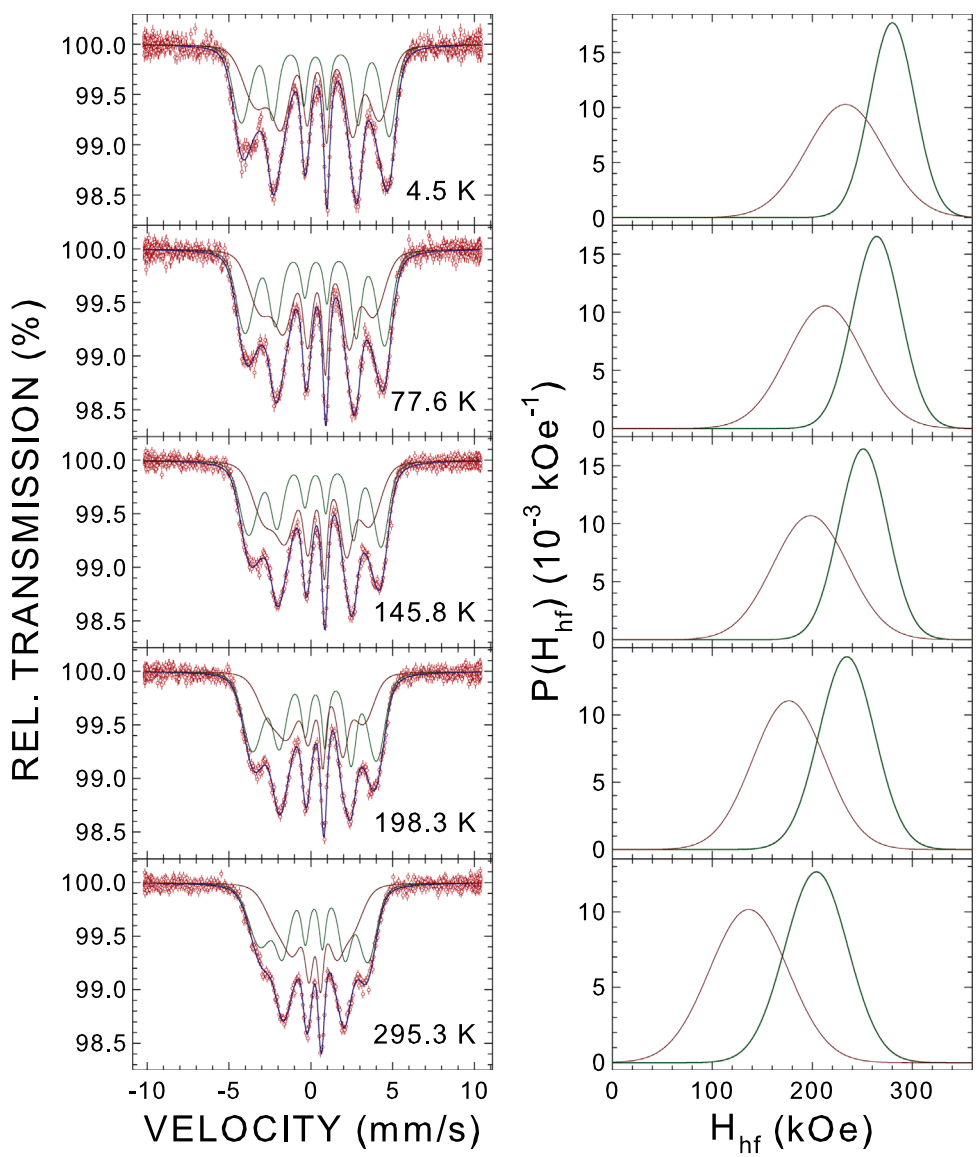

Fig. 8. ^{57}Fe Mössbauer spectra of the Fe_2NiGa Mössbauer absorber (σ_{exp} = 21.9 mg/cm^2) at the indicated temperatures fitted (blue solid lines) (left panel) with the A-site and B-site (dark red and dark green solid lines) Zeeman patterns resulting from the hyperfine magnetic field distributions $P(H_{hf})$ (right panel). The zero-velocity origin is relative to α-Fe at room temperature. (For interpretation of the references to color in this figure caption, the reader is referred to the web version of this paper.)

The hyperfine magnetic field at the Mössbauer nucleus in a magnetically ordered material consists of three main contributions: the Fermi contact term H_c, the magnetic dipolar term, H_{dip}, and the orbital moment term, H_{orb} [16]. Of these, the first term is usually significantly larger in magnitude than the last two terms. The Fermi contact term is given by

$$H_c = \frac{8\pi}{3}\mu_B^2(\rho_\uparrow(0) - \rho_\downarrow(0)), \tag{2}$$

where $\rho_\uparrow(0)$ and $\rho_\downarrow(0)$ are the spin-up and spin-down densities at the Mössbauer nucleus, respectively. The magnitudes of H_c at the A and B sites in Fe_2NiGa calculated from Eq. (2) are $H_c(A) = 166$ kOe and $H_c(B) = 260$ kOe.

3.3. Mössbauer spectroscopy

The room- and low-temperature ^{57}Fe Mössbauer spectra of Fe_2NiGa (Fig. 8) are in a form of significantly broadened Zeeman patterns that are very similar to the patterns observed for Fe-containing amorphous alloys [25]. These spectra clearly must result from the presence of a distribution $P(H_{hf})$ of the hyperfine magnetic fields H_{hf} at the A- and B-sites. This distribution originates from significant structural disorder present in the compound studied. Good fits of these spectra (left panel of Fig. 8) were obtained with the distributions [26] $P(H_{hf})$ at the A- and B-sites shown in the right panel of Fig. 8.

Fig. 9 shows the first series of consecutively measured high-temperature ^{57}Fe Mössbauer spectra of Fe_2NiGa. One observes that the last spectrum of this series measured at 300.2 K and its corresponding distributions $P(H_{hf})$ are very different from the 300.2 K spectrum and the corresponding distributions measured at the beginning of this series. This indicates that the specimen studied must have decomposed at ~500 K.

In the second series of consecutively measured high-temperature ^{57}Fe Mössbauer spectra (Fig. 10), the first high-temperature spectrum was measured at 600.2 K. It is in the form of a single line which indicates that the Curie temperature T_C of Fe_2NiGa must be smaller than 600.2 K. Similar to the first series, the last 300.2 K spectrum and the corresponding distributions $P(H_{hf})$ are very different from the 300.2 K spectrum and its distributions measured at the beginning of the second series (Fig. 10). This confirms that the studied compound decomposes when heated above ~500 K.

The average values of the hyperfine magnetic field at the A and B sites, $\overline{H}_{hf}(A)$ and $\overline{H}_{hf}(B)$, at a given temperature were calculated from the corresponding $P(H_{hf})$ distributions at that temperature (Figs. 8–10). The temperature dependence of $\overline{H}_{hf}(A)$ and $\overline{H}_{hf}(B)$ is presented in Fig. 11. One notices a strong, almost linear decrease of $\overline{H}_{hf}(A)$ and $\overline{H}_{hf}(B)$ with increasing temperature and a sudden disappearance of $\overline{H}_{hf}(A)$ and $\overline{H}_{hf}(B)$ above ~560 K. This unusual temperature dependence of $\overline{H}_{hf}(A)$ and $\overline{H}_{hf}(B)$ could be fitted neither to a Brillouin function [27] nor to a Bean–Rodbell function [28]. The Curie temperature $T_C = 580.2(20.0)$ K was estimated from the observation (Fig. 11) that $\overline{H}_{hf}(A) \neq 0$ and $\overline{H}_{hf}(B) \neq 0$ at 560.2 K, but $\overline{H}_{hf}(A) = \overline{H}_{hf}(B) = 0$ at 600.2 K.

The saturation values of the hyperfine magnetic field

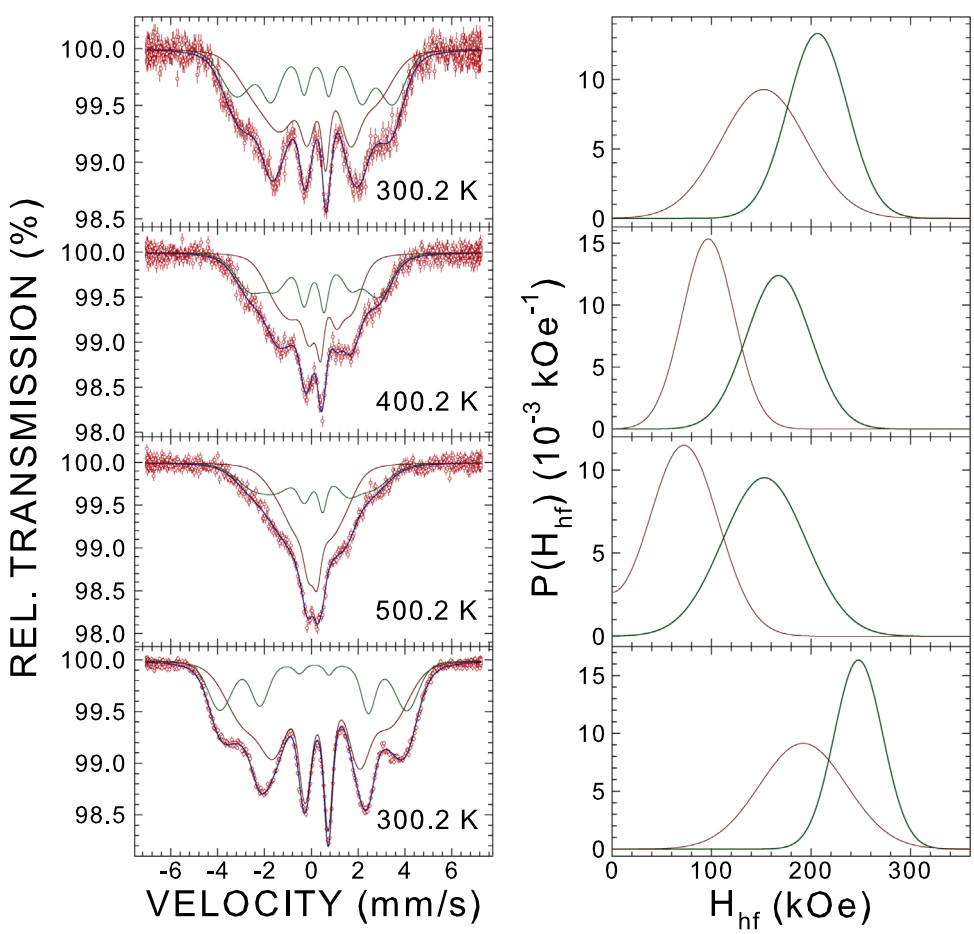

Fig. 9. ^{57}Fe Mössbauer spectra of the Fe_2NiGa Mössbauer absorber ($\sigma_{exp} = 21.6$ mg/cm^2) at the indicated temperatures fitted (blue solid lines) (left panel) with the A-site and B-site (dark red and dark green solid lines) Zeeman patterns resulting from the hyperfine magnetic field distributions $P(H_{hf})$ (right panel). The spectra were measured consecutively starting with the spectrum at 300.2 K (top left column) down to the spectrum at 300.2 K (bottom left column). The zero-velocity origin is relative to α-Fe at room temperature. (For interpretation of the references to color in this figure caption, the reader is referred to the web version of this paper.)

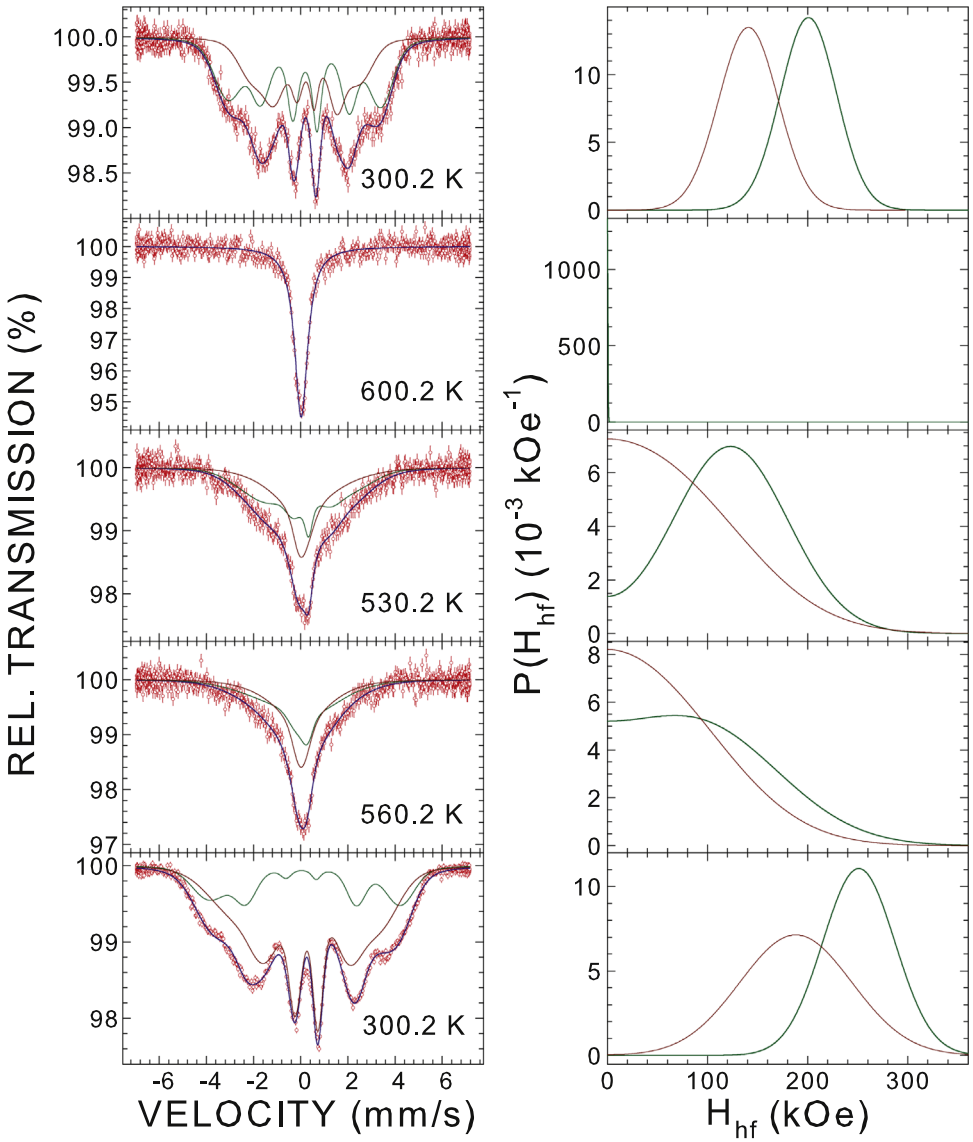

Fig. 10. ^{57}Fe Mössbauer spectra of the Fe_2NiGa Mössbauer absorber (σ_{exp} = 33.0 mg/cm^2) at the indicated temperatures fitted (blue solid lines) (left panel) with the A-site and B-site (dark red and dark green solid lines) Zeeman patterns resulting from the hyperfine magnetic field distributions $P(H_{hf})$ (right panel). The spectra were measured consecutively starting with the spectrum at 300.2 K (top left column) down to the spectrum at 300.2 K (bottom left column). The zero-velocity origin is relative to α-Fe at room temperature. (For interpretation of the references to color in this figure caption, the reader is referred to the web version of this paper.)

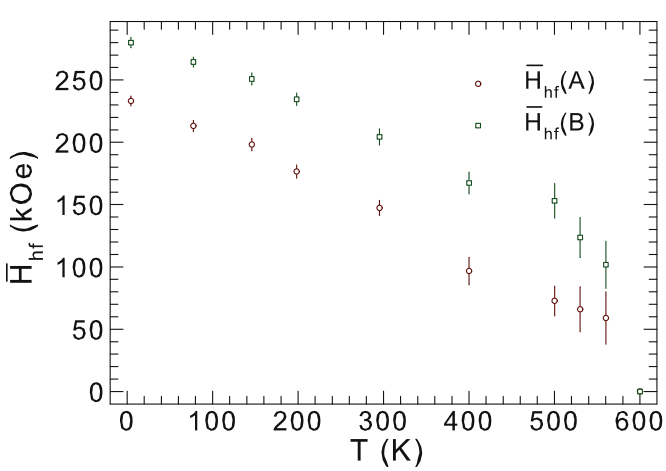

Fig. 11. Temperature dependence of the average hyperfine magnetic fields $\overline{H}_{hf}(A)$ and $\overline{H}_{hf}(B)$.

$\overline{H}_{hf,0}(A) = 234.3(2.2)$ kOe and $\overline{H}_{hf,0}(B) = 280.9(2.1)$ kOe were obtained from a linear extrapolation of the $\overline{H}_{hf}(A)$ and $\overline{H}_{hf}(B)$ data to 0 K (Fig. 11). The experimental values of $\overline{H}_{hf,0}(A)$ and $\overline{H}_{hf,0}(B)$ found here are higher, respectively, by 41% and 8.0% than the calculated $H_c(A)$ and $H_c(B)$ contributions. This confirms a general observation of the $|H_{dip} + H_{orb}|$ contribution being smaller in magnitude than the H_c contribution.

To a first approximation, H_{hf} is proportional to the on-site magnetic moment of iron atoms μ_{Fe} through the relation $H_{hf} = a\mu_{Fe}$, where the value of the proportionality constant a is compound specific [29]. In converting H_{hf} to μ_{Fe}, the value $a = 125$ kOe/μ_B was used [7]. Thus, the experimental $\overline{H}_{hf,0}(A)$ and $\overline{H}_{hf,0}(B)$ values correspond to $\overline{\mu}_{Fe,0}(A) = 1.87(2)\mu_B$ and $\overline{\mu}_{Fe,0}(B) = 2.25(2)\mu_B$, respectively. These values of $\overline{\mu}_{Fe,0}(A)$ and $\overline{\mu}_{Fe,0}(B)$ are only 4% and 16% lower than the calculated $\mu_{Fe}(A) = 1.941\mu_B$ and $\mu_{Fe}(B) = 2.680\mu_B$, respectively. It would be useful to estimate the experimental value of μ_{Ni} in Fe_2NiGa from the ^{61}Ni Mössbauer measurements [30] and compare it with the calculated value of $0.492\mu_B$.

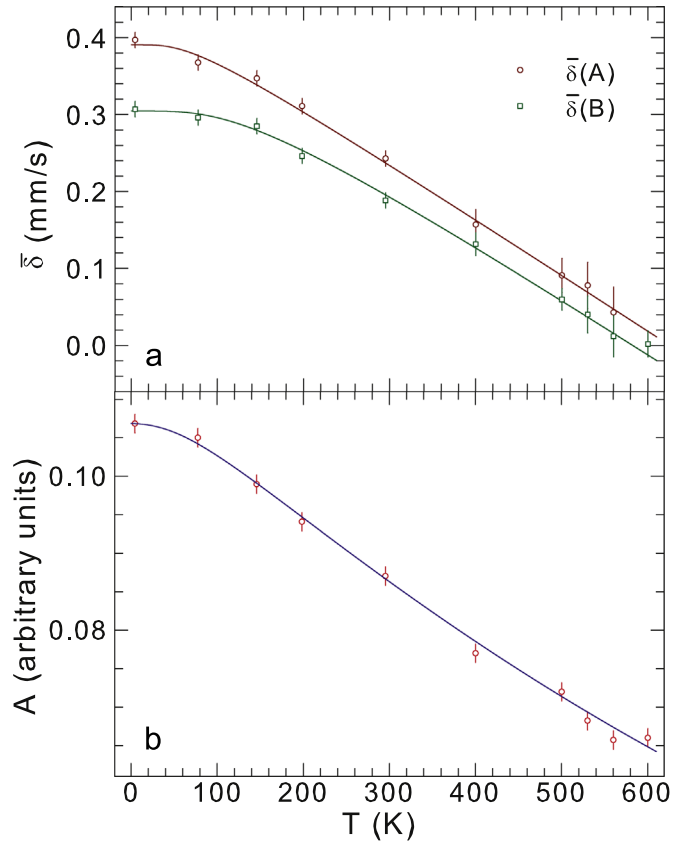

Fig. 12. Temperature dependence of (a) the average center shifts $\bar{\delta}(A)$ and $\bar{\delta}(B)$ and (b) the absorption spectral area A. The solid lines are the fits to Eq. (1) in (a) and to Eq. (3) in (b), as explained in the text.

The temperature dependence of the average values of the center shift at the A and B sites (relative to α-Fe at 298 K), $\bar{\delta}$(A) and $\bar{\delta}$(B), determined from the fits of the Mössbauer spectra in Figs. 8–10, is shown in Fig. 12(a). The $\delta(T)$ dependence is given by

$$\delta(T) = \delta_0 + \delta_{SOD}(T), \tag{3}$$

where δ_0 is the intrinsic isomer shift and $\delta_{SOD}(T)$ is the second-order Doppler (SOD) shift which depends on the lattice vibrations of the Fe atoms [16]. In terms of the Debye approximation of the lattice vibrations, $\delta_{SOD}(T)$ is expressed in terms of the Debye temperature Θ_D as

$$\delta_{SOD}(T) = -\frac{9}{2}\frac{k_B T}{Mc}\left(\frac{T}{\Theta_D}\right)^3 \int_0^{\Theta_D/T} \frac{x^3 dx}{e^x - 1}, \tag{4}$$

where M is the mass of the Mössbauer nucleus and c is the speed of light. By fitting the temperature dependence of $\bar{\delta}$(A) and $\bar{\delta}$(B) (Fig. 12) to Eq. (3), the quantities $\delta_0(A) = 0.391(9)$ mm/s, $\Theta_D(A) = 256(15)$ K and $\delta_0(B) = 0.305(8)$ mm/s, $\Theta_D(B) = 498(14)$ K were determined. The experimental value of $\delta_0(A)$ determined here is quite close to the calculated value of 0.361 mm/s. However, the experimental value of $\delta_0(B)$ is significantly larger than the calculated value of 0.180 mm/s. The observed inequality $\Theta_D(A) < \Theta_D(B)$ is indicative of a much larger bonding strength of the Fe atoms at the B sites than at the A sites. This conclusion can also be deduced from Fig. 4 where one can observe a higher degree of overlap between FeB and Ni states in comparison to that of FeA and Ni states. The Debye temperature of Fe_2NiGa calculated as the weighted average of $\Theta_D(A)$ and $\Theta_D(B)$ is then 385(10) K.

There is a second method of determining the Debye temperature from Mössbauer spectroscopy data. Fig. 12(b) displays the temperature dependence of the σ_{exp} – normalized absorption spectral area A derived from the fits of the Mössbauer spectra in Figs. 8–10. This area is proportional to the absorber Debye–Waller factor f_a, which is given in the Debye theory by [16]

$$f_a(T) = \exp\left\{-\frac{3}{4}\frac{E_\gamma^2}{Mc^2 k_B \Theta_D}\left[1 + 4\left(\frac{T}{\Theta_D}\right)^2 \int_0^{\Theta_D/T} \frac{x dx}{e^x - 1}\right]\right\}, \tag{5}$$

where E_γ is the energy of the Mössbauer transition. The fit of the experimental dependence $A(T)$ [Fig. 12(b)] to Eq. (5) yields $\Theta_D = 374(6)$ K. The weighted average of the above two Θ_D values determined from the temperature dependence of two different physical parameters is 378(5) K. This value is 11% lower than the calculated $\Theta_D = 427$ K.

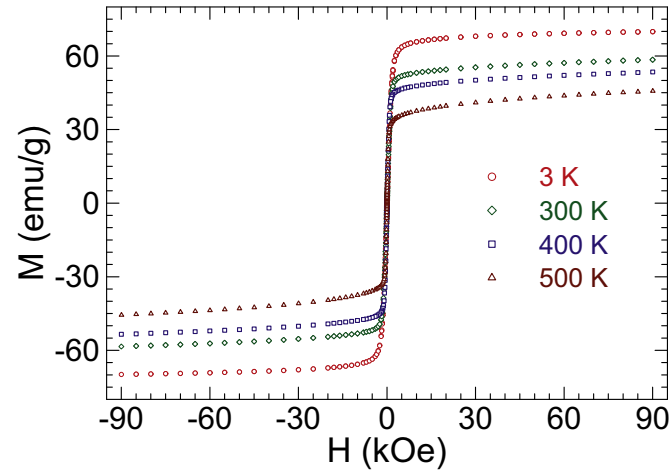

Fig. 13. Hysteresis curves of Fe_2NiGa at selected temperatures in the magnetic field range −90 to +90 kOe.

3.4. Magnetic measurements

The magnetic field dependence of magnetization curves $M(H)$ measured at selected temperatures (Fig. 13) are typical for a ferromagnet. They show that M at 3 K saturates in the highest field available of 90 kOe. The value of M at 3 K in that field is 69.86 emu/g ($3.00\mu_B$/f. u.). This value of $3.00\mu_B$/f. u. is significantly lower than the calculated $\mu_{fu} = 4.958\mu_B$ and the experimental values of $4.89\mu_B$/f. u. reported in Ref. [5] and $4.20\mu_B$/f. u. reported in Ref. [7].

In order to determine the Curie temperature T_C of the Fe_2NiGa ferromagnet, the temperature dependence of the magnetic susceptibility χ in external magnetic fields of 10 and 100 Oe was

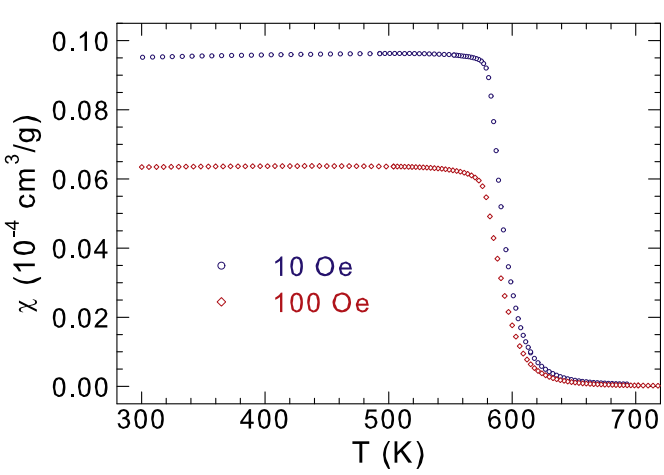

Fig. 14. Temperature dependence of the magnetic susceptibility of Fe_2NiGa measured in external magnetic fields of 10 and 100 Oe.

measured (Fig. 14). If one uses the definition of T_C as the temperature where the $\chi(T)$ curve has an inflection point (Fig. 14), then T_C is 587(1) K [585(1) K] as determined from the 10 Oe [100 Oe] $\chi(T)$ curves. It is thus concluded that the $\chi(T)$ data indicate that $T_C = 586.0(7)$ K. This value of T_C is close to the less-precise value of 580.2(20.0) K estimated from the $\overline{H}_{hf}(T)$ data. We note that our $T_C = 586.0(7)$ K is significantly smaller than $T_C = 785$ K reported in Ref. [5] (specimen annealed at 925 K for three days) or $T_C = 845$ K reported in Ref. [7] (specimen annealed at 673 K for two weeks). As the specimen studied here was annealed at 1073 K for two weeks, this wide spread of T_C and μ_{fu} is indicative of a dramatic influence of heat treatment on magnetism of the Heusler compound Fe_2NiGa.

4. Conclusions

The results of X-ray diffraction, ^{57}Fe Mössbauer spectroscopy, and magnetic measurements and of *ab initio* calculations of the electronic, magnetic, and hyperfine-interaction properties of Fe_2NiGa are presented. Both the X-ray diffraction spectrum and the Mössbauer spectra indicate the presence of significant structural disorder in the compound studied. It is predicted that Fe_2NiGa is half-metallic with covalent chemical bonding. It is demonstrated that Fe_2NiGa is a ferromagnet with the Curie temperature $T_C = 586.0(7)$ K. The Fe magnetic moments at the A and B sites estimated at 0 K and the saturation magnetization per formula unit are, respectively, 1.87(2), 2.25(2), and $3.00\mu_B$. We find that *ab initio* calculations overestimate the Fe magnetic moments. It is observed that different heat treatments of Fe_2NiGa result in its dramatically different magnetic properties. There is a reasonable agreement between the calculated and measured hyperfine-interaction parameters. We find that the Debye temperature of Fe_2NiGa is 378(5) K. It is observed that the compound studied decomposes when heated and kept at temperatures above around 500 K.

Acknowledgments

This work was supported by the Natural Sciences and Engineering Research Council of Canada.

References

[1] T. Graf, J. Winterlik, L. Müchler, G.H. Fecher, C. Felser, S.S.P. Parkin, in: K.H. J. Buschow (Ed.), Handbook of Magnetic Materials, vol. 21, Elsevier, Amsterdam, 2013, p. 1.
[2] T. Graf, C. Felser, S.S.P. Parkin, Prog. Solid State Chem. 39 (2011) 1 , and references therein.
[3] G.E. Bacon, J.S. Plant, J. Phys. F 1 (1971) 524.
[4] G. Kreiner, A. Kalache, S. Hausdorf, V. Alijani, J.-F. Qian, G. Shan, U. Burkhardt, S. Quardi, C. Felser, Z. Anorg. Allg. Chem. 640 (2014) 738.
[5] Y.J. Zhang, W.H. Wang, H.G. Zhang, E.K. Liu, R.S. Ma, G.H. Wu, Physica B 420 (2013) 86.
[6] J. Kiss, S. Chadov, G.H. Fecher, C. Felser, Phys. Rev. B 87 (2013) 224403.
[7] T. Gasi, V. Ksenofontov, J. Kiss, S. Chadov, A.K. Nayak, M. Nicklas, J. Winterlik, M. Schwall, P. Klaer, P. Adler, C. Felser, Phys. Rev. B 87 (2013) 064411.
[8] M. Gilleßen, R. Dronkowski, J. Comput. Chem. 31 (2010) 612.
[9] S.E. Kulkova, S.S. Kulkov, A.V. Subashiev, Comput. Mater. Sci. 36 (2006) 249.
[10] S.E. Kulkova, S.V. Eremev, S.S. Kulkov, Solid State Commun. 130 (2004) 793.
[11] M. Yin, S. Chen, Intermetallics 57 (2015) 34.
[12] E.S. Popiel, W. Zarek, M. Tuszyński, Nukleonika 49 (2004) S49.
[13] N. Kawamiya, K. Adachi, J. Magn. Magn. Mater. 31–34 (1983) 145.
[14] K.H.J. Buschow, P.G. Van Engen, J. Magn. Magn. Mater. 25 (1981) 90.
[15] Certificate of Calibration, in: J.P. Cali (Ed.) Iron Foil Mössbauer Standard, Natl. Bur. Stand. (U.S.) Circ. No. 1541, U.S. GPO, Washington, D.C., 1971.
[16] N.N. Greenwood, T.C. Gibb, Mössbauer Spectroscopy, Chapman and Hall, London, 1971;
P. Gütlich, E. Bill, A. Trautwein, Mössbauer Spectroscopy and Transition Metal Chemistry, Springer, Berlin, 2011.
[17] S. Margulies, J.R. Ehrman, Nucl. Instrum. Methods 12 (1961) 131;
G.K. Shenoy, J.M. Friedt, H. Maletta, S.L. Ruby, in: I.J. Gruverman, C.W. Seidel, D. K. Dieterly (Eds.), Mössbauer Effect Methodology, vol. 10, Plenum, New York, 1974, p. 277.
[18] P. Blaha, K. Schwartz, G. Madsen, D. Kvasnicka, J. Luitz, WIEN2k, An Augmented Plane Wave Plus Local Orbitals Program for Calculating Crystal Properties, Karlheinz Schwarz, Technical Universität Wien, Austria, 1999.
[19] J.P. Perdew, S. Burke, M. Ernzerhof, Phys. Rev. Lett. 77 (1996) 3865.
[20] R.A. Young, The Rietveld Method, Oxford University Press, Oxford, 1993.
[21] One notices a difference between the calculated μ_{fu} and the expected value of $\mu_{Fe(A)} + \mu_{Fe(B)} + \mu_{Ni} + \mu_{Ga}$. This is due to a non-zero magnetic moment of the interstitial region ($-0.101\ \mu_B$) which results from the leakage of a small amount of valence charge from the MT region into the interstitial region. This presence of charge in the interstitial region can also be taken as evidence for covalent nature of chemical bonding.
[22] O.L. Anderson, J. Phys. Chem. Solids 24 (1963) 909.
[23] P. Blaha, J. Phys.: Conf. Series 217 (2010) 012009.
[24] U.D. Wdowik, K. Reubenbauer, Phys. Rev. B 76 (2007) 155118.
[25] Z.M. Stadnik, G. Stroink, Hyperfine Interact. 47 (1989) 275.
[26] D.G. Rancourt, J.Y. Ping, Nucl. Instrum. Methods Phys. Res. B 58 (1991) 85.
[27] M.A. Albedah, F. Nejadsattari, Z.M. Stadnik, J. Przewoźnik, J. Alloys Compd. 613 (2014) 344.
[28] F. Nejadsattari, Z.M. Stadnik, J. Żukrowski, J. Alloys Compd. 639 (2015) 547.
[29] P. Panissod, J. Durand, J.I. Budnik, Nucl. Instrum. Methods 199 (1982) 99;
P. Panissod, Hyperfine Interact. 24–26 (1985) 607;
O. Eriksson, A. Svane, J. Phys.: Condens. Matter 1 (1989) 1589;
S.M. Dubiel, J. Alloys Compd. 488 (2009) 18.
[30] Z.M. Stadnik, P. Wang, N. Jansen, D. Walcher, P. Gütlich, T. Kanomata, J. Phys.: Condens. Matter 20 (2008) 325230;
Z.M. Stadnik, P. Griebach, G. Dehe, P. Gütlich, G. Stroink, T. Miyazaki, Phys. Rev. B 35 (1987) 8740.